The 12th IEEE International Workshop on Advanced Motion Control
March 25-27, 2012, Sarajevo, Bosnia and Herzegovina

A Coordinate Design of Two-Degrees-Of-Freedom Controller for Fast and Precise Positioning

Takanori Kato, Yoshihiro Maeda, Makoto Iwasaki, and Hiromu Hirai
Department of Computer Science and Engineering,
Nagoya Institute of Technology, Gokiso, Showa, Nagoya, 4668555, JAPAN
Email: kato.takanori@nitech.ac.jp

***Abstract*—This paper presents a novel robust 2-degrees-of-freedom (2-DOF) positioning controller design methodology against frequency perturbations in mechanical vibration modes. The authors have already proposed an LMI (linear matrix inequality)-based feedforward (FF) compensator design to provide robust properties in positioning against the perturbations, where a feedback (FB) controller has been independently designed to ensure the robust stability on the basis of the 2-DOF controller design framework. A problem, however, still remains that the undesired response in the FB system due to the perturbations deteriorates the ideal response by the FF compensation. The proposed controller design, therefore, considers the FB system in the FF compensator design to solve the problem. In addition, the FB controller is redesigned to improve the positioning performance as a coordinate design between the FB and the FF controllers. The effectiveness of the proposed approach has been verified by numerical simulations and experiments using a prototype of galvano scanners.**

I. Introduction

Fast response and high-precision positioning is one of indispensable techniques in a wide variety of high performance mechatronic systems, such as data storage devices, machine tools, and industrial robots [1]. In the positioning devices with mechanical vibration modes, however, the positioning performance is deteriorated by perturbations in the mode frequencies due to aging and/or environment variations [2].

A 2-DOF control framework is one of promising approaches to achieve robust properties against the perturbations [3], [4], [5], [6]. The authors have already proposed an LMI-based FF compensator design to ensure the robust properties against the resonance frequency perturbations, where the specified constrains on state variables, such as control input and/or position responses, can be directly determined by the LMI optimization framework [7]. In the conventional design, however, the positioning performance is deteriorated by the FB control loop, since the undesired responses in the FB system due to the perturbation affect the ideal response by the FF compensation.

In this research, therefore, a novel coordinate design between the FF and FB controllers of the 2-DOF positioning system is proposed to improve the robustness against the resonance frequency perturbations. The proposed design considers the FB control property with the perturbations to solve the problem in the conventional method. Under the consideration, the FB controller is redesigned to prevent the undesired response characteristic and to improve the total positioning performance of the 2-DOF control system. The effectiveness of the proposed controller design has been verified by numerical simulations and experiments using a prototype of galvano scanners in industrial laser manufacturing applications.

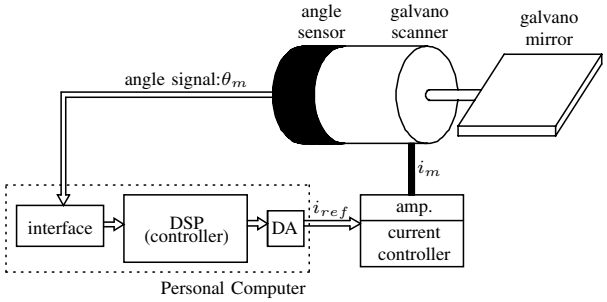

Fig. 1. Configuration of experimental setup.

II. Positioning System of Galvano Scanner

A. Configuration of Positioning Device

Fig.1 shows a configuration of a positioning device for galvano scanners as an experimental setup. The galvano scanner is composed of a servo motor with a galvano mirror, where the motor angle θ_m is directly detected by a rotary encoder and transfered to a DSP controller through an interface. The servo motor is driven by a current controlled amplifier with the current reference i_{ref} generated by the position controller, where the position controller calculates the current reference as the control input with the sapling period T_s of 20 μs.

Light red lines in Fig.2 show a Bode characteristic of θ_m for i_{ref}, where the environment temperature around the galvano scanner is kept in 25 degrees centigrade as nominal condition in the following controller design. The mechanism includes the primary vibration mode at 2.95 kHz, the second vibration mode at 5.95 kHz, the third vibration mode at 6.25 kHz, other vibration modes in the high frequency range, and a dead time component due to the current control delay. A nominal plant model $P_n(s)$ is formulated as follows, consisting of a rigid mode, vibration modes up to $i = 3$, and a dead time component:

$$P_n(s) = \frac{\theta_m(s)}{i_{ref}(s)} = e^{-Ls} K_p \left(\frac{1}{s^2} + \sum_{i=1}^{3} \frac{k_i}{s^2 + 2\zeta_i \omega_i s + \omega_i^2} \right), \quad (1)$$

978-1-4577-1073-5/12/$26.00 ©2012 IEEE

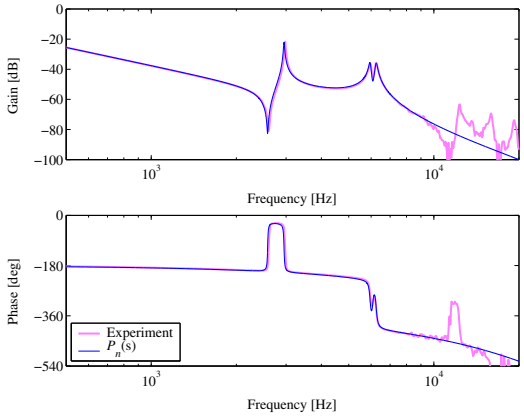

Fig. 2. Bode characteristics of plant system.

TABLE I
PARAMETERS OF PLANT MODEL.

K_p	1.82 $\times 10^4$	L	1.32 $\times 10^{-5}$ s
k_1	0.42	ω_1	$2\pi\times$ 2950 rad/s
k_2	-0.75	ω_2	$2\pi\times$ 5950 rad/s
k_3	-0.95	ω_3	$2\pi\times$ 6250 rad/s
ζ_1	4.0 $\times 10^{-3}$	ζ_2	9.0 $\times 10^{-3}$
ζ_3	10.0 $\times 10^{-3}$		

where K_p: gain including moment of inertia, torque constant of motor and current controller, ω_i: natural angular frequency of i-th vibration mode, ζ_i: damping coefficient, k_i: vibration mode gain, and L: equivalent dead time, respectively. Paramters of a nominal plant model $P_n(s)$ are shown in Table I. Dark blue lines in Fig.2 indicate a Bode characteristic of $P_n(s)$. From the figure, the mathematical model can well express the actual characteristic, except in the high frequency range more than 10 kHz.

B. Target Positioning Specification

In this research, a position reference with amplitude of 1.5 mm is given as one of the typical control specifications for the laser manufacturing, where the position should be settled within the accuracy of ± 2.5 μm with the settling time of 0.76 ms ($= 38T_s$). Notice here that, in this positioning device, since the resonance frequency of the primary vibration mode may be varied in the maximum ± 100 Hz due to the environment and/or temperature fluctuations, the robust position controller against the perturbation is required to satisfy the target control specifications.

C. 2-DOF Position Control System

Fig.3 shows a block diagram of the 2-DOF position control system based on the final state control [5], where $P(z)$: plant, $C(z)$: FB compensator, u^*: FF control input, u: control input ($= i_{ref}$), y: motor position ($= \theta_m$), r: target motor position trajectory reference, and e: trajectory error, respectively. The FB compensator $C(z)$ consists of a phase lag-lead compensator and two notch filters as follows, considering

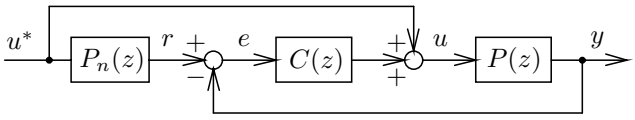

Fig. 3. Block diagram of 2-DOF position control system.

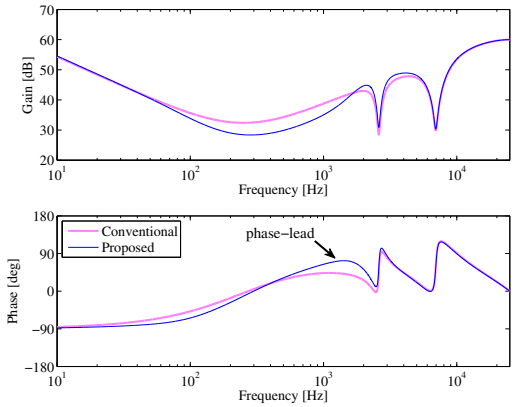

Fig. 4. Bode characteristics of FB compensators.

the disturbance suppression capability and the robust stability against the resonance frequency perturbation:

$$C(s) = K_c \frac{s+\omega_{c1}}{s} \frac{s+\omega_{c3}}{s+\omega_{c2}} \prod_{i=1}^{2} \frac{s^2+2\zeta_{ni}\omega_{ni}s+\omega_{ni}^2}{s^2+2\zeta_{di}\omega_{ni}s+\omega_{ni}^2}. \quad (2)$$

In the controller implementation of the DSP, $C(s)$ of eq.(2) is transformed to $C(z)$ by a tustin transformation. Light red lines in Fig.4 show a Bode characteristic of $C(z)$.

III. CONVENTIONAL FF COMPENSATION DESIGN

A. Design Model

Plant model in the conventional design is an augmented system which includes the nominal plant model and uncertainties by the resonance frequency perturbation, to consider the robustness against the perturbation in the FF control input. Fig.5 shows a block diagram of the design model, where $P_n(s)$: nominal plant of eq.(1), $\Delta(s)$: uncertainty by the plant perturbation, $\mathcal{H}$: zeroth-order hold, $\frac{1}{z-1}$: integrator, y_n: nominal position response ($y_n = P_n(s)u^*$), y_e: varied position response ($y_e = \Delta(s)u^*$), and u_d^*: jerk in the FF control input, respectively. State expressions of $P_n(s)$ and $\Delta(s)$ are formulated as follows:

- Nominal plant model $P_n(s)$:

$$\begin{bmatrix} \dot{\boldsymbol{x}}_n \\ y_n \end{bmatrix} = \begin{bmatrix} \boldsymbol{A}_n & \boldsymbol{B}_n \\ \boldsymbol{C}_n & D_n \end{bmatrix} \begin{bmatrix} \boldsymbol{x}_n \\ u^* \end{bmatrix}, \quad (3)$$

- Uncertainty of plant $\Delta(s)$:

$$\begin{bmatrix} \dot{\boldsymbol{x}}_e \\ y_e \end{bmatrix} = \begin{bmatrix} \boldsymbol{A}_e & \boldsymbol{B}_e \\ \boldsymbol{C}_e & D_e \end{bmatrix} \begin{bmatrix} \boldsymbol{x}_e \\ u^* \end{bmatrix}, \quad (4)$$

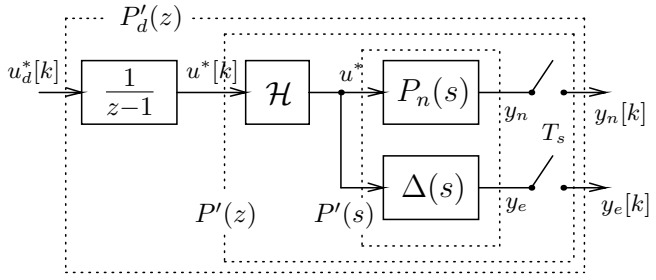

Fig. 5. Block diagram of augmented system with plant perturbation in conventional design.

where $\boldsymbol{A}_n$∼$\boldsymbol{D}_n$: state matrices of $P_n(s)$, $\boldsymbol{A}_e$∼$\boldsymbol{D}_e$: state matrices of $\Delta(s)$, $\boldsymbol{x}_n \in R^{8\times1}$: state variable of $P_n(s)$, and $\boldsymbol{x}_e \in R^{2\times1}$: state variable of $\Delta(s)$, respectively. The augmented system $P'(s)$ in Fig.5, on the other hand, can be defined as follows:

$$\begin{bmatrix} \dot{\boldsymbol{x}}' \\ \boldsymbol{y}' \end{bmatrix} = \begin{bmatrix} \boldsymbol{A}' & \boldsymbol{B}' \\ \boldsymbol{C}' & \boldsymbol{D}' \end{bmatrix} \begin{bmatrix} \boldsymbol{x}' \\ u^* \end{bmatrix}, \tag{5}$$

where $\boldsymbol{x}'$, $\boldsymbol{y}'$, $\boldsymbol{A}'$, $\boldsymbol{B}'$, $\boldsymbol{C}'$, and $\boldsymbol{D}'$ are given as:

$$\boldsymbol{x}' = \begin{bmatrix} \boldsymbol{x}_n^T & \boldsymbol{x}_e^T \end{bmatrix}^T \in R^{10\times1},\ \boldsymbol{y}' = \begin{bmatrix} y_n & y_e \end{bmatrix}^T \in R^{2\times1},$$
$$\boldsymbol{A}' = \begin{bmatrix} \boldsymbol{A}_n & \boldsymbol{O} \\ \boldsymbol{O} & \boldsymbol{A}_e \end{bmatrix} \in R^{10\times10},\ \boldsymbol{B}' = \begin{bmatrix} \boldsymbol{B}_n^T & \boldsymbol{B}_e^T \end{bmatrix}^T \in R^{10\times1},$$
$$\boldsymbol{C}' = \begin{bmatrix} \boldsymbol{C}_n & \boldsymbol{O} \\ \boldsymbol{O} & \boldsymbol{C}_e \end{bmatrix} \in R^{1\times10},\ \boldsymbol{D}' = \begin{bmatrix} D_n & D_e \end{bmatrix}^T \in R^{2\times1}.$$

Discrete augmented system $P'_d(z)$ in Fig.5 can be represented as follows, including an integrator to attenuate the jerk u^*_d [8]:

$$\begin{bmatrix} \boldsymbol{x}'[k+1] \\ u^*[k+1] \\ \boldsymbol{y}'[k] \end{bmatrix} = \begin{bmatrix} \boldsymbol{A}'_d & \boldsymbol{B}'_d & \boldsymbol{O} \\ \boldsymbol{O} & 1 & 1 \\ \boldsymbol{C}'_d & \boldsymbol{D}'_d & \boldsymbol{O} \end{bmatrix} \begin{bmatrix} \boldsymbol{x}'[k] \\ u^*[k] \\ u^*_d[k] \end{bmatrix}, \tag{6}$$

where $\boldsymbol{A}'_d$∼$\boldsymbol{D}'_d$ are discrete matrices for $\boldsymbol{A}'$∼$\boldsymbol{D}'$ by zeroth-order hold.

B. LMI-Based FF Compensation Design

In the LMI-based FF compensation design, the following FF control input is calculated, on the basis of the final state control:

$$\boldsymbol{u}^* = \begin{bmatrix} u^*[0] & \cdots & u^*[N-1] \end{bmatrix}^T \in R^{N\times1}. \tag{7}$$

At first, in order to design $\boldsymbol{u}^*$ which ensures to settle the nominal response y_n to the target position X_r by N steps from the initial state $\boldsymbol{x}[0]$ of zero, the final state condition can be given as:

$$\boldsymbol{x}_n[N] = \begin{bmatrix} X_r & 0 & 0 & 0 & 0 & 0 & 0 & 0 \end{bmatrix}^T \in R^{8\times1}, \tag{8}$$

where X_r and N are determined as $X_r = 1.5$ mm and $N = 38$, to achieve the target positioning specification. The state constraints, therefore, can be given by the following matrix equation as an affine function of $\boldsymbol{u}^*_{\boldsymbol{d}}$:

$$\begin{aligned} \boldsymbol{\Sigma}\boldsymbol{u}^*_d &= \boldsymbol{x}[N], \\ \boldsymbol{\Sigma} &= \begin{bmatrix} \boldsymbol{A}_d'^{N-1}\boldsymbol{B}'_d, & \boldsymbol{A}_d'^{N-2}\boldsymbol{B}'_d, & \cdots & \boldsymbol{B}'_d \end{bmatrix}. \end{aligned} \tag{9}$$

Then, in order to avoid the saturation of the control input, $\boldsymbol{u}^*_d$ can be designed by considering the input amplitude of $\boldsymbol{u}^*$ by the following inequality constraint:

$$-u_m < u^*[k] < u_m \qquad (k = 1, \cdots, N), \tag{10}$$

where the maximum amplitude u_m is given as of 8 V considering the maximum control input of ±10 V. In addition, the varied response y_e can be restricted as follows, to allow y_e to be settled with the specified settling accuracy of $\pm y_m$ μm:

$$-y_m < y_e[k] < y_m \quad (k = N-2, \cdots, N+35). \tag{11}$$

In this research, two uncertainties (+100 Hz and −100 Hz in ω_1) as the resonance frequency perturbations of the primary mode are defined in the design model, while the inequality constraint of eq.(11) is adopted to the varied response with $y_m = 2.5$ μm.

Finally, the FF control input $\boldsymbol{u}^*$ in Fig.5 which satisfies the constraints of eqs.(9)∼(11) is optimized under the following cost function, on the basis of the LMI technique [9]:

$$J = \sum_{k=0}^{N-1} u^*_d[k]^2. \tag{12}$$

C. Subjects of Conventional Approach

Subjects of the conventional FF compensation design are clarified by positioning simulations of $X_r = 1.5$ mm stroke. Fig.6 shows the simulated response waveforms of (a) FF control input u^* and (b) position error $X_r - y$, where dark blue solid lines (Nominal) indicate nominal responses and light red solid lines (ω_1: −100 Hz) indicate varied responses by the resonance frequency perturbation ($\omega_1 = 2\pi \times 2850$ rad/s). In the case of the nominal condition, amplitude of the FF control input in Fig.6 (a) can be restricted within the

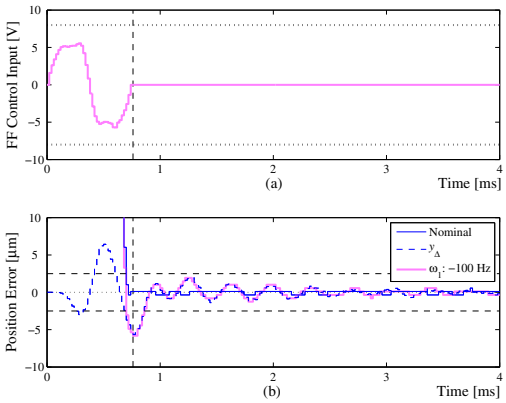

Fig. 6. Simulated response waveforms by conventional design.

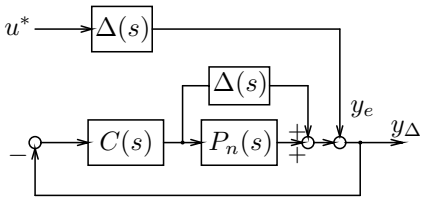

Fig. 7. Block diagram of error model.

limitation of ± 8 V indicated by horizontal dotted lines, while the position response settles to the target position by $N = 38$ steps, satisfying the target control specification. In the case of with the resonance frequency perturbation, on the other hand, the overshoot response which cannot satisfy the constraint on the settling accuracy of ± 2.5 μm by eq.(11) occurs immediately after the settling, resulting in the deterioration of the positioning performance. In order to examine why the varied position response proceeds the constraint of eq.(11), a block diagram of error model including $\Delta(s)$ in Fig.7 is introduced. From the figure, the error response y_Δ can be given as:

$$y_\Delta = \frac{1}{1 + C(s)\{P_n(s) + \Delta(s)\}} y_e \tag{13}$$

$$= \frac{1}{1 + C(s)\{P_n(s) + \Delta(s)\}} \Delta(s) u^*. \tag{14}$$

From eq.(14), the error response y_Δ can be expressed by the error response y_e of the FF compensation as well as the response by the FB control system. That is, the response deterioration in Fig.6 may be caused by the FB system, since the conventional approach does not consider the effect of the FB control. Dark blue dashed line in Fig.6 shows a response waveform of y_Δ with the perturbation. Notice here that, the summation of y_n and y_Δ corresponds to y. From the figure, since y_Δ exceeds the settling accuracy of $\pm$ 2.5 μm, the response by the FB control system deteriorates the positioning performance in the conventional approach. Therefore, in order to provide the better robust positioning performance better than the conventional approach, the effect of the FB system should be simultaneously considered in the FF compensation design.

IV. Coordinate Design of 2-DOF Controller

From the examinations on the error response in III-C, the proposed approach as "coordinate design of the FF and FB controllers", includes the FB control system with the plant perturbation in the design model of the FF compensation design, to apply the constraint of eq.(11) to the position response strictly. Then, considering that the FB controller affects the LMI-based FF compensation design in the proposed approach, the FB controller is redesigned on the basis of the error response characteristic to improve the positioning performance.

A. Proposed Design Model

Fig.8 shows a block diagram of the proposed design model $P''(s)$. In the proposed approach, $P''(s)$ considers the FB

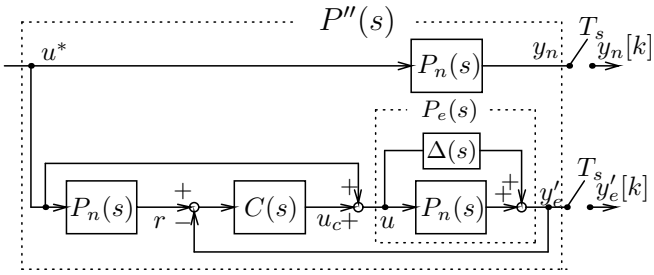

Fig. 8. Block diagram of augmented system with FB compensator.

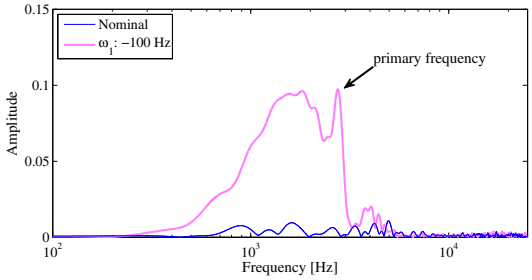

Fig. 9. Frequency spectrums of error response.

control system with the uncertainty of the plant, instead of $P'(s)$ in Fig.5. In Fig.8, the space expressions of the FB compensator $C(s)$ and the closed-loop system are formulated as follows:

- FB compensator $C(s)$:

$$\begin{bmatrix} \dot{\boldsymbol{x}}_c \\ u_c \end{bmatrix} = \begin{bmatrix} \boldsymbol{A}_c & \boldsymbol{B}_c \\ \boldsymbol{C}_c & D_c \end{bmatrix} \begin{bmatrix} \boldsymbol{x}_c \\ r - y_e \end{bmatrix}, \tag{15}$$

- Closed-loop system:

$$\begin{bmatrix} \dot{\boldsymbol{x}}_{cl} \\ y'_e \end{bmatrix} = \begin{bmatrix} \boldsymbol{A}_{cl} & \boldsymbol{B}_{cl} \\ \boldsymbol{C}_{cl} & D_{cl} \end{bmatrix} \begin{bmatrix} \boldsymbol{x}_{cl} \\ u^* \end{bmatrix}, \tag{16}$$

where $\boldsymbol{A}_{cl}$, $\boldsymbol{B}_{cl}$, $\boldsymbol{C}_{cl}$, D_{cl}, and $\boldsymbol{x}_{cl}$ are given as:

$$\boldsymbol{A}_{cl} = \begin{bmatrix} \boldsymbol{A}_n & \boldsymbol{O} & \boldsymbol{O} \\ \boldsymbol{B}_c\boldsymbol{C}_n & \boldsymbol{A}_c & -\boldsymbol{B}_c\boldsymbol{C}_e \\ \boldsymbol{B}_e D_c \boldsymbol{C}_n & \boldsymbol{B}_e\boldsymbol{C}_c & \boldsymbol{A}_e - \boldsymbol{B}_e D_c \boldsymbol{C}_e \end{bmatrix},$$

$$\boldsymbol{B}_{cl} = \begin{bmatrix} \boldsymbol{B}_n \\ \boldsymbol{O} \\ \boldsymbol{B}_e \end{bmatrix}, \qquad \boldsymbol{C}_{cl} = \begin{bmatrix} \boldsymbol{O} & \boldsymbol{O} & \boldsymbol{C}_e \end{bmatrix},$$

$$D_{cl} = 0, \qquad \boldsymbol{x}_{cl} = \begin{bmatrix} \boldsymbol{x}_n^T & \boldsymbol{x}_c^T & \boldsymbol{x}_e^T \end{bmatrix}^T \in R^{22\times 1}.$$

In the proposed approach, the varied position response y'_e in eq.(16) is restricted in the same manner as in eq.(11), and the proposed FF control input can be designed by the same way as of the conventional approach in III-B. In this research, we call this proposed design as "Proposed 1" in the following.

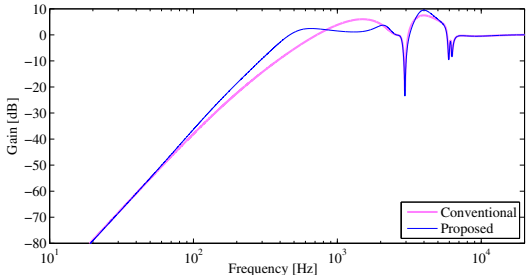

Fig. 10. Gains of sensitivity characteristics.

B. FB Compensator Considering Sensitivity Function

As the coordinate design of 2-DOF controllers, the FB controller is redesigned to improve the positioning performance, considering the error response y_Δ. Fig.9 shows frequency spectrums of error response y_Δ in Fig.6, where dark blue line (Nominal) indicates a spectrum in the nominal condition and light red line (ω_1: -100 Hz) indicates the one with the resonance frequency perturbation. In the case with the perturbation, the primary vibration component by the perturbation as well as in the frequency range of 1∼2 kHz which corresponds to the servo bandwidth is increased comparing to the nominal condition. From eq.(14), the increase of the component in 1∼2 kHz may be caused by the sensitivity characteristic of the FB control system. The light red line in Fig.10 shows the gain characteristic of the sensitivity function by the conventional FB controller $C(s)$. From Fig.10, the gain is above zero dB in the frequency range of 1∼2 kHz, resulting in the increase of the error response in the corresponding frequency range.

Proposed FB controller $C'(s)$, therefore, modifies the conventional FB controller $C(s)$ by adding filters as follows, to improve the sensitivity properties:

$$C'(s) = C(s) \cdot \prod_{i=1}^{2} \frac{s^2 + 2\zeta_{nri}\omega_{nri}s + \omega_{nri}^2}{s^2 + 2\zeta_{dri}\omega_{dri}s + \omega_{dri}^2}. \tag{17}$$

The add-on filters are designed as phase-lead elements in the range of 1∼2 kHz, while the stability margin and the disturbance suppression capability are ensured as of the conventional ones. Dark blue lines in Fig.4 shows a Bode diagram of the proposed FB controller $C'(s)$. From the figure, the phase leads in the frequency range of 1∼2 kHz comparing to $C(s)$, which keeps the same gain level equivalent in the low frequency. Dark blue line in Fig.10 shows a gain characteristic of the sensitivity by $C'(s)$. From Fig.10, the proposed controller realizes the gain reduction of the sensitivity in the frequency of 1∼2 kHz, keeping the disturbance suppression capability in the low frequency up to 100 Hz. In the following, we call this proposed design as "Proposed 2".

C. Simulation Verifications

The effectiveness of the proposed coordinate design is verified by numerical simulations. The FF control input is designed under the limitation y_m in eq.(11) as of $y_m = 1.5$ μm.

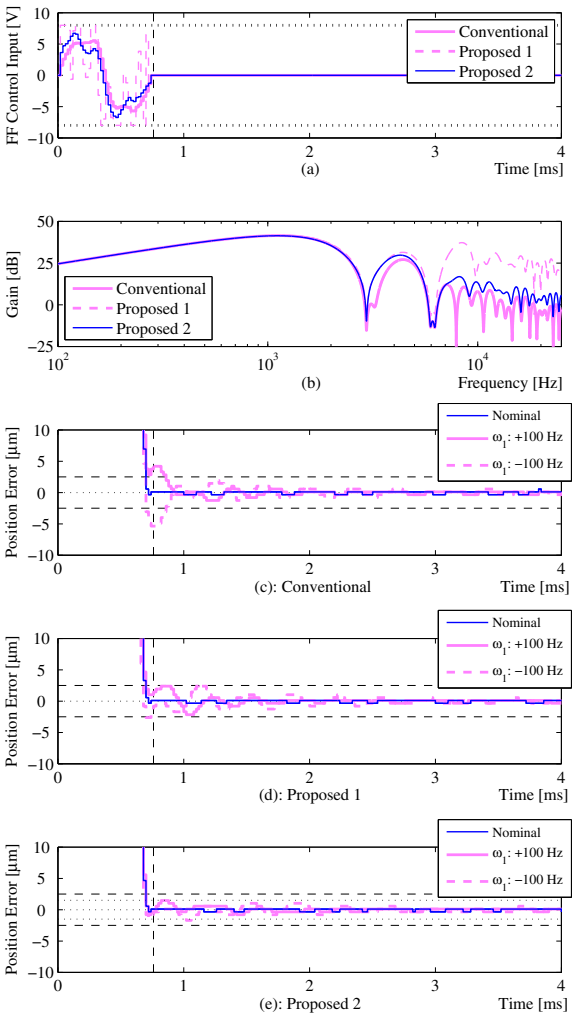

Fig. 11. Simulated response waveforms by conventional and proposed method.

Fig.11 shows simulated response waveforms of (a) FF control input, (b) frequency spectrum of the FF control input, (c) position error by the conventional method, (d) position error by "Proposed 1", and (e) position error by "Proposed 2". In (a) and (b), light red solid lines (Conventional) indicate the conventional design, light red dashed lines ("Proposed 1") indicate "Proposed 1", and dark blue solid lines ("Proposed 2") indicate "Proposed 2". In (c), (d), and (e), dark blue solid lines (Nominal) indicate the nominal condition, light red solid and dashed lines (ω_1: $\pm$100 Hz) indicate with the perturbations. In the conventional design, the FF control input is restricted within $\pm$8 V by the constraint of eq.(10), while the frequency spectrum is suppressed at around the primary vibration mode. In cases of the perturbations, however, over/undershoot responses which proceed the target accuracy of $\pm$2.5 μm occur immediately after the settling, which cannot satisfy the constraint of eq.(11) by the horizontal

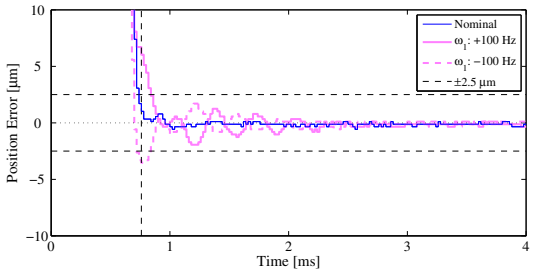

(a): Conventional

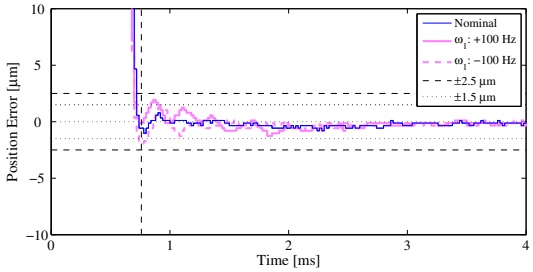

(b): Proposed 2

Fig. 12. Experimental response waveforms by conventioinal and proposed method.

dashed lines. In "Proposed 1", over/undershoot responses are suppressed under the constraint of eq.(11) by considering the FB control system in the LMI-based FF compensation design model. The FF control input, however, includes high frequency components remarkably, since the FB control system amplifies the component in 1∼2 kHz which cannot be suppressed by the FF compensation. In "Proposed 2", on the other hand, over/undershoot and vibration responses are well-suppressed within the constraint of eq.(11) ($y_m = 1.5$ μm) indicated by horizontal dotted lines by considering the effect of the sensitivity characteristic on the error response y_Δ. In addition, the high frequency component in the FF control input can be decreased significantly decreased comparing to "Proposed 1", since the component of the error response in the frequency range of 1∼2 kHz is effectively suppressed by the proposed FB controller.

V. Experimental verifications

The proposed coordinate design has been verified by experiments using a prototype. In experiments, frequency perturbations are simulated by fluctuating the primary vibration frequency of the nominal plant model $P_n(z)$ in the FF compensation [4]. Fig.12 shows experimental response waveforms of (a) position error by the conventional design, (b) position error by "Proposed 2", where dark blue lines indicate the case of the nominal condition, light red solid and broken lines (ω_1: $\pm$100 Hz) indicate the ones with the perturbations. In the conventional design, the over/undershoot responses proceeding the target accuracy of $\pm$ 2.5 μm indicated by horizontal broken lines ($\pm$ 2.5 μm) are caused by the perturbations, as in the same manner as in the simulations of Fig.11. In "Proposed 2", on the other hand, although each varied responses due to perturbations are slightly proceeded the constraint indicated by horizontal dotted lines ($\pm$1.5 μm), over/undershoot responses are well-suppressed, achieving the target positioning specification.

VI. Conclusions

In this paper, the coordinate design between the FF and FB compensators in the 2-DOF positioning system is proposed to provide the robustness against frequency perturbations. The proposed approach can ensure the desired robust control performance by giving the constraints in the LMI framework. In addition, the FF and FB compensators are coordinated to improve the positioning performance by considering the error response due to the perturbation, realizing the required robust positioning. The effectiveness of the proposed approach has been verified by numerical simulations and experiments using the positioning device of the galvano scanner.

References

[1] S. Katsura, K. Irie, and K. Ohishi: "Wideband Force Control by Position-Acceleration Integrated Disturbance Observer", *IEEE Trans. on Industrial Electronics*, Vol.55, No.4, pp.1699-1706, 2008

[2] K. Ohno, and T. Hara: "Adaptive Resonant Mode Compensation for Hard Disk Drives", *IEEE Trans. on Industrial Electronics*, Vol.53, No.2, pp.624-630, 2006

[3] K. Saiki, A. Hara, K. Sakata, and H. Fujimoto: "A Study on High-Speed and High-Precision Tracking Control of Large-Scale Stage Using Perfect Tracking Control Method Based on Multirate Feedforward Control", *IEEE Trans. on Industrial Electronics*, Vol.57, No.4, pp.1393-1400, 2010

[4] N. Hirose, M. Iwasaki, M. Kawafuku, and H. Hirai: "Deadbeat Feedforward Compensation With Frequency Shaping in Fast and Precise Positioning", *IEEE Trans. on Industrial Electronics*, Vol.56, No.10, pp.3790-3797, 2009

[5] M. Hirata, and F. Ueno: "Final-State Control Using Polynomial and Time-Series Data", *IEEE Trans. on Magnetics*, Vol.47, No.7, pp.1944-1950, 2011

[6] T. Kato, Y. Maeda, M. Iwasaki, and H. Hirai: "LMI-Based 2-Degrees-Of-Freedom Controller Design for Robust Vibration Suppression Positioning", *T. IEE Japan*, Vol.131, No.1, pp.93-101, 2011 (in Japanese)

[7] K. Ito, M. Yamamoto, M. Iwasaki, and N. Matsui: "LMI-Based Robust Command Shaping Against Plant Perturbations in Fast and Precise Positioning", Proc. of ICROS-SICE International Joint Conference, Fukuoka, pp.13-18, 2009

[8] Y. Mizoshita, S. Hasegawa, and K. Takaishi: "Vibration Minimized Access Control For Disk Drives", *IEEE Trans. on Magnetics*, Vol.32, No.3, pp.1793-1798, 1996

[9] M. Yamamoto, M. Iwasaki, S. Mitsuhashi, K. Ito, and N. Matsui: "Robust Position Command Shaping against Plant Perturbations under Constraint of State Variables", *T. IEE Japan*, Vol.129, No.7, pp.714-724, 2009 (in Japanese)

[10] T. Atsumi, A. Okuyama, and M. Kobayashi: "Track-Following Control Using Resonant Filter in Hard Disk Drives", *IEEE/ASME Trans. on Mechatronics*, Vol.12, No.4, pp.472-479, 2007

[11] J. Zheng, M. Fu, C. Du, Y. Wang, and L. Xie: "A Factorization Approach to Sensitivity Loop Shaping for Disturbance Rejection in Hard Disk Drives", *IEEE Trans. on Magnetics*, Vol.46, No.5, pp.1220-1227, 2010